*Original Article*

Acta Radiologica
0(0) 1–8

DOI: 10.1177/0284185115574156
acr.sagepub.com
SAGE

# Is there a role for conventional MRI and MR diffusion-weighted imaging for distinction of skull base chordoma and chondrosarcoma?

**Uta Müller[1], Rahel A Kubik-Huch[1], Carmen Ares[2], Eugen B Hug[3], Roland Löw[1], Antonios Valavanis[4] and Frank J Ahlhelm[1]**

## Abstract

**Background:** Chordoma and chondrosarcoma are locally invasive skull base tumors with similar clinical symptoms and anatomic imaging features as reported in the literature.

**Purpose:** To determine differentiation of chordoma and chondrosarcoma of the skull base with conventional magnetic resonance imaging (cMRI) and diffusion-weighted MR imaging (DWI) in comparison to histopathological diagnosis.

**Material and Methods:** This retrospective study comprised 96 (chordoma, $n = 64$; chondrosarcoma, $n = 32$) patients with skull base tumors referred to the Paul Scherrer Institute (PSI) for proton therapy. cMRI signal intensities of all tumors were investigated. In addition, median apparent diffusion coefficient (ADC) values were measured in a subgroup of 19 patients (chordoma, $n = 11$; chondrosarcoma, $n = 8$).

**Results:** The majority 81.2% (26/32) of chondrosarcomas displayed an off-midline growth pattern, 18.8% (6/32) showed clival invasion, 18.8% (6/32) were located more centrally. Only 4.7% (3/64) of chordomas revealed a lateral clival origin. Using cMRI no significant differences in MR signal intensities were observed in contrast to significantly different ADC values (subgroup of 19/96 patients examined by DWI), with the highest mean value of $2017.2 \times 10^{-6}\,mm^2/s$ (SD, $139.9\,mm^2/s$) for chondrosarcoma and significantly lower value of $1263.5 \times 10^{-6}\,mm^2/s$ (SD, $100.2 \times 10^{-6}\,mm^2/s$) for chordoma ($P = 0.001$/median test).

**Conclusion:** An off-midline growth pattern can differentiate chondrosarcoma from chordoma on cMRI in a majority of patients. Additional DWI is a promising tool for the differentiation of these skull base tumors.

**Keywords**
Magnetic resonance imaging (MRI), diffusion-weighted MRI (DWI), ADC map, chordoma, chondrosarcoma, skull base tumor

Date received: 27 October 2014; accepted: 18 January 2015

## Introduction

Chordoma and chondrosarcoma are slow growing skull base tumors which are locally invasive and in direct vicinity of critical structures such as lower cranial nerves and internal carotid artery. The overall prognosis is poor as a result of local failure potency (1,2). The gold standard for treatment for these rare tumors is surgical excision and postoperative radiation therapy. Advances in skull base microsurgery, and radiation techniques, not limiting but including protons, provide promising opportunities for survival and long-term outcome (3,4).

Chordomas and chondrosarcomas are rare, generally slowly but invasively growing tumors. At the skull base, chordomas comprise about 0.15% of all

[1]Department of Radiology, Kantonsspital Baden AG, Switzerland
[2]Center for Proton Therapy, Paul Scherrer Institute, Villigen, Switzerland
[3]Princton Radiation Oncology Center, Monroe Township, NJ, USA
[4]Institute of Neuroradiology, University Hospital Zürich, Switzerland

**Corresponding author:**
Uta Müller, Department of Radiology, Kantonsspital Baden AG, Im Ergel 1, 5404 Baden, Switzerland.
Email: uta.muellerpfister@ksb.ch

primary intracranial neoplasms and 4% of all primary bone tumors, with chondrosarcomas making up only about 0.02% of all intracranial neoplasms (1,5–7).

Chordomas originate from primitive notochordal remnants and at the skull base are centrally located in the clivus, predominantly along the midline, sometimes slightly more lateral in the vicinity of the spheno-occipital synchondrosis (8). Primary malignant cartilaginous chondrosarcomas are thought to arise from primitive mesenchymal cells or from the embryonal rest of the cartilaginous matrix and usually occur in the area of the foramen lacerum adjacent to the spheno-petrosal, the petro-occipital, and the petro-clival synchondrosis (9). At the skull base the lesser malignant chondrosarcoma subtypes I and II are predominantly observed (10).

Since complete surgical tumor resection at the skull base is seldom achievable due to either adhesion or encasement of the adjacent critical neuronal and vascular structures, the major goal of surgery prior to radiotherapeutical treatment is gross surgical tumor debulking (1,11,12).

The histologic characteristics of these two entities have been described before. A histopathological example of each entity is shown in Fig. 1. Notable differences in the histopathologic appearance of these tumor entities can be seen microscopically and differentiation of these entities based on conventional MRI alone is reported to be not feasible since both tumors show similar signal intensities in T2-weighted (T2W) and T1-weighted (T1W) imaging and similar contrast media enhancement patterns (13). Furthermore, tumor extension does not allow for discrimination between chordoma and chondrosarcoma. In contrast to signal intensity using conventional MR sequences and tumor extent, the origin of the tumor might be an important indication for differential diagnosis.

Advanced MRI techniques such as diffusion-weighted imaging (DWI) and hence calculation of the apparent diffusion coefficient (ADC) is promising for many applications, including oncology – for example, to detect early recurrence after surgical resection of brain tumors or to evaluate suspicious lymph node metastases. There are only few papers in the literature discussing the role of DWI technique in discriminating chordomas and chondrosarcomas (14,15).

The aim of this study was to investigate if tumor localization and DWI combined with ADC calculation can contribute to and improve the preoperative differentiation between chordomas and chondrosarcomas.

## Material and Methods

Study authorization was given by the Institutional Review Board of our institute. Written informed consent was obtained from all patients.

The retrospective case study cohort comprised 96 patients (chordomas, $n = 64$; chondrosarcomas, $n = 32$) with histopathologically confirmed skull base tumors collected consecutively between January 2007 and December 2012. Patients underwent brain and skull base MRI in preparation for proton radiation therapy at the PSI. Proton therapy treatment planning and delivery is described in detail in an earlier publication by the PSI – radio-oncological group (3,4,16). Preoperative MRI acquired at the time of diagnosis of all patients provided by the PSI radiation oncologist was re-evaluated by consensus by three board-certified neuroradiologists with more than 10 years of experience in MRI. As expected, presurgical initial imaging was performed on different scanner models because of the worldwide patient referral. MRIs were investigated for the epicenter of tumor origin, the detailed anatomy involved, signal intensities as well as DWI including calculation of the apparent diffusion coefficient (ADC) if available. For invasion grading the clivus was virtually fragmented into six parts. Three parallel-oriented zones

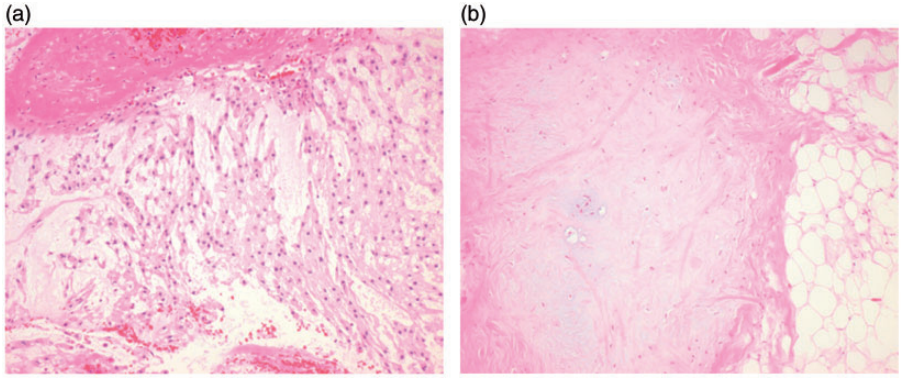


**Fig. 1.** Tumor histopathology. (a) Classic chordoma. Areas showing groups of cells with small round nuclei and partly vacuolated cytoplasm are sometimes referred to as physalipherous. Cell nests separated by fibrous septa are embedded in a myxoid tumor matrix. (b) Chondrosarcoma grade I. Small groups of malignant chondrocytes in a chondroid tumor matrix.

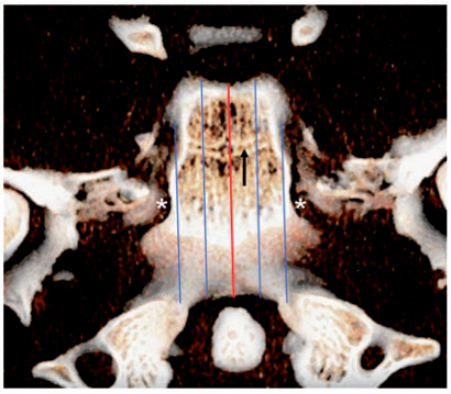

**Fig. 2.** Skull base anatomy. Axial plane: infant skull base – CT volume rendering technique (VRT) reconstruction. Definition of three parallel-oriented zones (blue lines) to each side of the clival midline (red line) to evaluate the extent of clival tumor erosion. Arrow: spheno-occipital synchondrosis. Asterisk: petro-occipital (petroclival) synchondrosis.

to each side of the clival midline were defined as shown in Fig. 2.

In a subgroup of 19 patients (chordoma, $n = 11$; chondrosarcoma, $n = 8$), additional DWI was available for measurements of ADC. ADC maps were generated with commercially available software from the echo-planar DW images, using at least three different b-values in the Stejskal-Tanner equation (17,18). To evaluate the validity of the measurements two differently sized round regions of interest (ROI) within each tumor of the subgroup were randomly placed and drawn manually on axial plane images in a blinded fashion to both pathologic and clinical information. ROIs were positioned within the tumor matrix, excluding regions of macroscopic cysts, calcification, necrosis, potential intratumoral hemorrhage, and/or mucinous parts identified in the anatomic T2W as well as T2*W and susceptibility-weighted sequences.

MRI features were compared to the histopathologic diagnosis. The chi-square test was used to compare differences in patient's characteristics. Associations between the histopathologic diagnosis and MRI features, as well as tumor location, were statistically assessed with Fisher's exact test and mean averaged ADC values of the DWI with Mood's median test. A $P$ value $<0.05$ was considered statistically significant. The statistical analyses were performed with the commercially available Statistical Package for the Social Sciences (SPSS Inc., Chicago, IL, USA).

## Results

Ninety-seven consecutive patients with skull base chordoma and chondrosarcoma were identified from our Picture archive and communicating system (PACS) database. Patient characteristics are summarized in Table 1.

**Table 1.** Patient characteristics.

| Patient characteristics | Chordoma ($n = 64$) | Chondrosarcoma ($n = 32$) | Total ($n = 96$) |
|---|---|---|---|
| *Gender* | | | |
| Male | 35 | 10 | 45 |
| Female | 29 | 22 | 51 |
| Male:Female ratio | 1.21/1 | 0.45/1 | 0.88/1 |
| Age (years) | | | |
| Mean ± SD | 50 ± 16.3 | 45 ± 14.2 | 48 ± 15.7 |
| <48 | 24 | 19 | 43 |
| >48 | 40 | 13 | 53 |
| Range | 13–80 | 20–67 | 13–80 |
| Histology | | | |
| | 62 classic type<br>2 chondroid type | 26 grade I<br>6 grade II | |

The age was significantly different between both patient groups ($P = 0.042$).

One patient with a histopathology of chordoma was excluded because of a potential epipharyngeal tumor origin with secondary destruction of the clivus. In a subgroup of 19 patients DWI and ADC maps were available.

The mean age of the chordoma subgroup ($n = 64$) was 50 years (age range, 13–80 years) at the time of tumor diagnosis in comparison to 45 years (age range, 20–67 years) in the chondrosarcoma subgroup ($n = 32$). The male-to-female ratio was 35/29 (1.21/1) for the chordoma patients versus 10/22 (0.45/1) for the chondrosarcoma patients. Chi-square statistic: 4.128; $P = 0.042$.

Histopathology revealed 62 classic chordomas, two chondroid chordomas, 26 grade 1 chondrosarcomas, and six grade 2 chondrosarcomas.

### *Tumor localization*

Tumors were assessed for their potential site of origin and invasion of surrounding structures. An overview of involved anatomical structures is given in Table 1.

Within the chordoma group, none of the cases presented with less than one-third clival transverse invasion. Six of 32 (18.8%) showed less than one-sixth transverse fraction clival invasion, and 9/32 (28.1%) less than one-third of the transverse clival plane.

In total, 61/64 chordomas (95.3%) showed midline clival growth. 10/64 (15.6%) with additional left and 14/64 (21.9%) with additional right-sided involvement. Only 6/32 (18.8%) chondrosarcomas revealed the

**Table 2.** Tumor localization.

| Tumor localization | Chordoma ($n=64$) (%) | Chondrosarcoma ($n=32$) (%) | Total ($n=96$) (%) |
|---|---|---|---|
| Clivus midline growth | 61 (95.3%) | 6 (18.8%) | 67 (69.8%) |
| Left extension | 10 (15.6%) | 14 (43.8%) | 24 (25.0%) |
| Right extension | 14 (21.9%) | 12 (37.5%) | 26 (27.1%) |
| Erosion < 17% | 0 | 6 (18.8%) | |
| Erosion < 33% | 0 | 9 (28.1%) | |
| Cavernous sinus | | | |
| Bilateral growth | 24 (37.5%) | 2 (6.3%) | 26 (27.1%) |
| Left extension | 9 (14.1%) | 13 (40.6%) | 22 (22.9%) |
| Right extension | 11 (17.2%) | 8 (25%) | 19 (20.8%) |
| Sphenoid sinus | 40 (62.5%) | 13 (40.6%) | 53 (55.2%) |
| Petrous bone | | | |
| Bilateral growth | 7 (10.9%) | 0 | |
| Left extension | 7 (10.0%) | 11 (34.4%) | 18 (18.7%) |
| Right extension | 11 (17.2%) | 11 (34.4%) | 22 (22.9%) |
| Prepontine Premedullary cistern | 55 (85.9%) | 14 (43.8%) | 69 (71.9%) |

same midline growth pattern. 14/32 (43.8%) of the chondrosarcomas were oriented to the left, 12/32 (37.5%) to the right.

Bilateral cavernous sinus extension within the laterosellar space was observed in 24/64 (37.5%) chordoma patients, versus only 2/32 (6.3%) of the chondrosarcoma patients. Bilateral petrosal bone invasion was only observed in 7/64 (22%) patients of the chordoma subgroup. Similar to the clival growth patterns, various orientations were observed concerning petrous invasion and prepontine extension, as shown in Table 2.

### *Conventional MRI signal characteristics*

In total, 92/96 (95.8%) of tumors showed hyperintense signal intensity compared to brain parenchyma in T2W imaging. Ninety of 96 (93.8%) of tumors revealed T1W hypointense signal intensities, 6/96 (6.3%) T1W showed partly hyperintense signal intensities due to intratumoral hemorrhage or mucinous components. In general, a mixed pattern of hyperintense signal intensities in T2W imaging in both tumor entities was observed without significant differences in signal intensities within both tumor types.

With respect to contrast media enhancement, there was no significant difference between the two tumor entities. Typical tumor examples are shown in Figs. 3 and 4.

### *Quantification of intra-tumoral apparent diffusion*

In a subgroup of 19 patients, DWI sequences and apparent diffusion coefficient (ADC) maps were available for patients with classic type chordoma and grade I chondrosarcoma.

Chordomas were associated with lower ADC values (mean ADC, $1263.5 +/- 100.2 \times 10^{-6}\,mm^2/s$) compared to chondrosarcomas with significant higher values (mean ADC, $2017.2 +/- 139.9 \times 10^{-6} mm^2/s$). ADC measurement results are presented in Table 3. Since the number of evaluated patients is small and two different intra-tumoral ROIs were measured an additional Mood's median test was performed ($P=0.001$). The median ADC value of all acquired ROIs of the two subgroups is $1268.1 \times 10^{-6}\,mm^2/s$ for the chordoma patients and $2051.7 \times 10^{-6}\,mm^2/s$ for the chondrosarcoma patients regarding a total number of 19 patients.

With a minimum size of $16.1\,mm^2$ there was no statistically significant intra-tumoral heterogeneity of ADC calculated for small and large regions of interest (maximum, $62.3\,mm^2$). Examples of intratumoral regions of interest (ROIs) are shown in Figs. 3 and 4.

## Discussion

The skull base represents a complex anatomical region and is within the scope of interest of a variety of clinical subspecialties, not only for the radiologist or neuroradiologist, but also since it represents historically the dividing line between surgical territories of the ear-nose-throat surgeon and the neurosurgeon. With improvements in radiation therapy such as proton beam radiation therapy, it is also the focus of attention of radiation-oncologists (3,4).

Because of their overlapping clinical symptoms and anatomic imaging features reported in the literature,

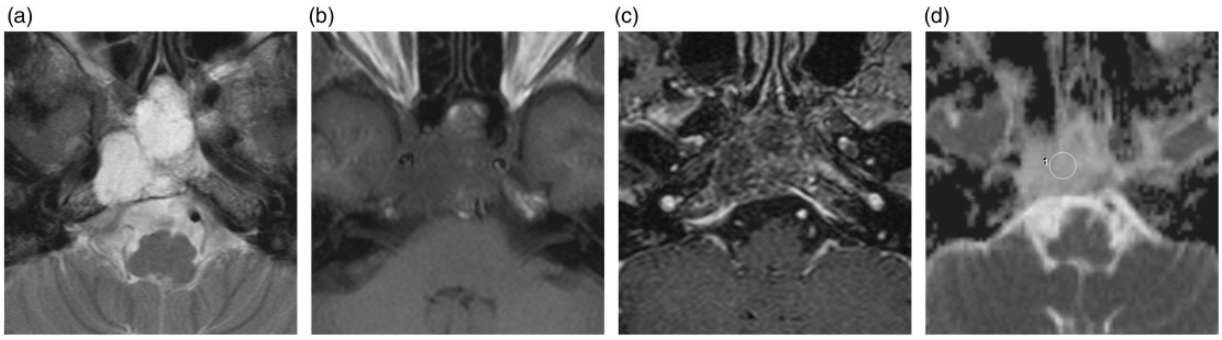


**Fig. 3.** Conventional MRI tumor example and ADC example of an intratumoral ROI in a patient with classic clival chordoma. (a) T2W axial plane: hyperintense mass with low-signal intensity septations separating high-signal intensity lobules. (b) T1W axial plane: hypointense to brain parenchyma with two subtle hyperintense linear areas at the anterior tumor margin consistent with mucinous and/or small hemorrhagic areas. A fatty component is not likely as a differential diagnosis within the tumor matrix. (c) T1W postcontrast axial plane: heterogeneous small-to-moderate contrast enhancement. (d) ADC map: intratumoral ROI 18.7 $mm^2$, mean ADC 1297.3 $\times 10^{-6}$ $mm^2/s$, SD 102.8 $\times 10^{-6}$ $mm^2/s$.

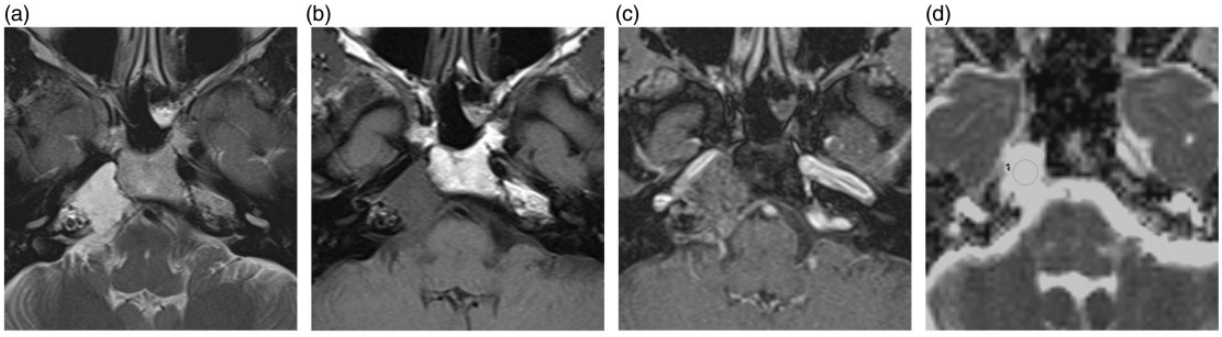


**Fig. 4.** Conventional MRI tumor example and ADC example of an intratumoral ROI in a patient with skull base chondrosarcoma. (a) T2W axial plane: hyperintense lobulated mass with dural invasion, extending posterior into the right prepontomedullary cistern. (b) T1W axial plane: homogeneous mass lesion hypointense to brain parenchyma. (c) T1W postcontrast axial plane: heterogeneous moderate contrast enhancement. (d) ADC map: intratumoral ROI 26.6 $mm^2$, mean ADC 1842.0 $\times 10^{-6}$ $mm^2/s$, SD 140.0 $\times 10^{-6}$ $mm^2/s$.

preoperative differentiation of chordomas and chondrosarcomas is difficult (19). Preoperative differentiation between the two entities is important not only for therapeutic considerations, but also for prognosis, since survival rates are worse for chordomas compared to chondrosarcomas (14,20,21).

To date, several articles describe the radiologic features of chordomas and chondrosarcomas, although most of the publications are limited by the small series of patients owing to the rarity of these tumors (11,14,19,22).

A study conducted in the 1970s reported that chondrosarcomas and chordomas exhibit different clinical behavior. In the present era clinical manifestation of symptoms is no longer considered a valid parameter for distinguishing between the two tumor entities (20).

Other previous studies have suggested that chondrosarcomas are diagnosed earlier in life compared with chordoma (19,23). Our study supports this statement because the median age at diagnosis of chondrosarcomas was 5 years earlier compared to chordoma, furthermore the age difference was significant ($P = 0.042$). However, both tumors can occur in childhood and early adult life. Hence, age at diagnosis is not a real reliable diagnostic parameter for differentiating these entities.

Although it is rather difficult to define the exact localization of origin of a chordoma or chondrosarcoma, the assumed site of tumor origin, i.e. midline origin or off-midline origin, seems to be an important indication according to our results. Chordomas are believed to arise from embryologic remnants of the notochord along the midline of the skull base at the spheno-occipital synchondrosis (8). Defining the exact origin is not always possible, since both tumors are able to invade the surrounding tissue in a rather unpredictable fashion. In our study, the primary limitation for defining the exact origin and distinguishing between the tumor entities was either left or right lateral tumor extension with respect to mid-clival growth. In all

**Table 3.** ADC values for tumors, comprising two different ROIs for each tumor (1–11: chordomas; 12–19: chondrosarcomas).

| Patient number | ROI size ($mm^2$) | Mean ADC ($\times 10^{-6} mm^2/s$) | SD ($\times 10^{-6} mm^2/s$) | Maximum ADC | Minimum ADC |
|---|---|---|---|---|---|
| 1 | 25.5 | 857.5 | 43.7 | 1120 | 997 |
| | 69.4 | 679.6 | 37.3 | 771 | 580 |
| 2 | 17.1 | 1035.3 | 95.9 | 1289 | 860 |
| | 31.5 | 1242.3 | 134.4 | 1501 | 1036 |
| 3 | 18.7 | 1429.4 | 138.4 | 1602 | 1047 |
| | 41.6 | 1241 | 125.6 | 1501 | 975 |
| 4 | 18.7 | 1016.7 | 121.4 | 1232 | 765 |
| | 18.7 | 1029.5 | 113.7 | 1290 | 845 |
| 5 | 20.3 | 1348.2 | 115.9 | 1549 | 1127 |
| | 37.5 | 1313.0 | 129.5 | 1529 | 1019 |
| 6 | 18.7 | 1265.2 | 91.4 | 1391 | 998 |
| | 63.1 | 1271.0 | 91.4 | 1487 | 951 |
| 7 | 15.8 | 1556.5 | 133.0 | 1745 | 1374 |
| | 17.2 | 1654.7 | 85.5 | 1772 | 1503 |
| 8 | 18.7 | 1618.0 | 76.0 | 1710 | 1490 |
| | 18.7 | 1610.0 | 105.0 | 1750 | 1400 |
| 9 | 16.1 | 1351.8 | 50.5 | 1425 | 1289 |
| | 42.0 | 1169.1 | 91.0 | 1342 | 1038 |
| 10 | 18.7 | 1297.3 | 102.8 | 1505 | 1116 |
| | 18.7 | 1282.8 | 92.2 | 1449 | 1107 |
| 11 | 10.5 | 1345.6 | 123.4 | 1519 | 1109 |
| | 15.8 | 1184.0 | 106.5 | 1409 | 1008 |
| **Mean** | | **1263.5** | 100.2 | 1449.5 | 1074.3 |
| 12 | 17.1 | 2139.0 | 145.3 | 2422 | 1925 |
| | 29.2 | 2255.2 | 87.0 | 2371 | 2090 |
| 13 | 23.4 | 1880.6 | 40.7 | 1958 | 1785 |
| | 59.7 | 1885.1 | 108.9 | 2319 | 1673 |
| 14 | 26.6 | 1842.0 | 140.0 | 2050 | 1510 |
| | 62.3 | 1645.0 | 135.0 | 1970 | 1410 |
| 15 | 34.7 | 1747.3 | 164.6 | 2078 | 1467 |
| | 52.6 | 1731.5 | 153.1 | 1980 | 1424 |
| 16 | 23.4 | 2032.0 | 129.0 | 2230 | 1840 |
| | 54.9 | 2086.0 | 83.0 | 2260 | 1890 |
| 17 | 23.4 | 2215.0 | 138.0 | 2490 | 1980 |
| | 54.9 | 2292.0 | 145.0 | 2590 | 2020 |
| 18 | 38.7 | 2491.0 | 137.0 | 2640 | 2190 |
| | 42.0 | 1945.0 | 161.0 | 2210 | 1580 |
| 19 | 23.4 | 1827.6 | 224.0 | 2200 | 1281 |
| | 35.5 | 2261.1 | 247.9 | 2678 | 1717 |
| **Mean** | | **2017.2** | 139.9 | 2277.8 | 1736.3 |

SD, standard deviation.

cases of the midline tumor growth of chondrosarcomas (6/32 patients), even repeated visual diagnostic assessment after 6 months, blinded to the histopathological diagnosis, did not lead to the right radiological diagnosis. In all other cases (90/96 patients) localization, i.e. midline or off-midline tumor origin, led to the right diagnosis. Controversial results are reported in literature (14,19,24). In contrast to our results

revealing tumor lateralization as a characteristic feature for differentiation between chordoma and chondrosarcoma, Yeom et al. – who examined only 19 patients with brain MRI – could not distinguish between the two entities by the location of the lesion (14). This might be explained by the small patient sample, which consisted of nine chondrosarcomas and 10 chordomas.

In a more recent study reported by Pamir et al. in 2006 investigating 42 skull base chordomas and chondrosarcomas, no difference in tumor extent or localization was revealed, which might also be explained by the low number ($n = 4$) of chondrosarcomas (19). There was also no difference with respect to lesion volume or tumor extent between the two chordoma subtypes, i.e. classic or chondroid. This is confirmed by our observations, but is limited since we also had only two cases of chondroid chordomas in our patient cohort.

Our findings concur with other reports, that MR signal intensities and contrast media enhancement of both tumors are not valid criteria for distinguishing between the two tumor entities (14,19).

DWI is quite a new functional MRI technique for assessing bone lesions, but has already shown its importance in stroke imaging, in other intracranial pathologic conditions such as the differentiation of edema and gliosis, as well as for diagnosis of primary brain tumors and other conditions, including abscess formation (25,26). With respect to bone metastasis, DWI is a sensitive method for detecting bone metastasis (27).

By calculating the ADC, which allows the quantitative determination of the apparent diffusion, it enables characterization of ischemic, inflammatory and neoplastic processes. For skull base lesions, Razek et al. reported that ADC calculation permits differentiation of malignant tumors from benign lesions and even the assessment of pathological grading of malignant tumors (28). In general, ADC values in benign skull base lesions are significantly higher compared to malignant lesions. Recently, Ginat et al. investigated the usefulness of DWI and cell density for differentiating benign from malignant skull lesions, showing that ADC correlated well with cell density and aided in the differential diagnoses for indeterminate skull lesions (15). An ADC threshold of $1010 \times 10^{-6}\,mm^2/s$ was reportedly optimal for differentiating benign lesions from malignancies. According to their results, malignant tumors showed significantly lower ADCs compared with benign lesions, with the exceptions of both chordoma and chondrosarcoma, which showed elevated ADC levels. However, their series only included one case of chordoma and two low-grade chondrosarcomas (28).

As reported for chondrosarcomas of the extremities, an ADC value of $2290 \times 10^{-6}\,mm^2/s$ in skull base chondrosarcomas is even higher than most benign lesions (15,29). This can be explained by the sparse cellularity of chondrosarcomas and chordomas. With respect to the differentiation between chordoma and chondrosarcoma of the skull base, Yeom et al. reported that DWI – and hence ADC calculation – is a promising technique for their distinction (14). With a highest mean ADC value of $2051 \times 10^{-6}\,mm^2/s$, chondrosarcoma of the clivus had apparent diffusion characteristics comparable with chondrosarcoma of the extremities. Classic chordoma had also been reported to be characterized by elevated ADCs, with a mean value of $1474 \times 10^{-6}\,mm^2/s$, which was significantly lower compared to chondrosarcoma (14).

In the present study chondrosarcomas also showed significantly higher apparent diffusion ($2170 \times 10^{-6}\,mm^2/s$) than chordomas ($1264 \times 10^{-6}\,mm^2/s$). The latter were near the threshold reported by Ginat et al. (15).

As a limitation of this study ADC parameter maps were not available for all patients in this study sample. Partially different b-values and different magnetic field strengths, different gradient rising times may also have a small influence of individual ADC quantification (30). However, ADC values of chordomas and chondrosarcomas already published by different groups fall into similar ranges and therefore seem to be reliable (14,15). Another hint for the reliability of the ADC measurements is the coherency of the blinded differently-sized ROIs within the same tumor with only small inter-individual variations. However, further studies on the reliability of ADC calculations and help to define of ADC- thresholds seem to be needed to discriminate these two tumor entities.

In conclusion, based on the present study, demonstration of a midline clival tumor strongly suggests the diagnosis of chordoma over chondrosarcoma, which tends to be located around the petro-occipital fissure. Furthermore, although no ADC value threshold could be determined, chondrosarcomas displayed significantly higher ADC values than chordomas. Compared with other malignancies and benign tumors of the skull base, chordoma and chondrosarcoma show less restricted diffusion.

## Conflict of interest

None declared.

## Funding

This research received no specific grant from any funding agency in the public, commercial, or not- commercial.

## Acknowledgements

We express our gratitude towards Dr G Goitein, former Clinical Director ad interim of the Centre for Proton

Therapy at the Paul Scherrer Institute in Switzerland, for her friendly advice during the research project.

## References


1. Gay E1, Sekhar LN, Rubinstein E, et al. Chordomas and chondrosarcomas of the cranial base: results and follow-up of 60 patients. Neurosurgery 1995;36:887–896.
2. Smoll NR, Gautschi OP, Radovanovic I, et al. Incidence and relative survival of chordomas: the standardized mortality ratio and the impact of chordomas on a population. Cancer 2013;119:2029–2037.
3. Rutz HP, Weber DC, Goitein G, et al. Postoperative spot-scanning proton radiation therapy for chordoma and chondrosarcoma in children and adolescents: initial experience at the Paul Scherrer Institute. Int J Radiat Oncol Biol Phys 2008;71:220–225.
4. Ares C, Hug EB, Lomax AJ, et al. Effectiveness and safety of spot scanning proton radiation therapy for chordomas and chondrosarcomas of the skull base: first long-term report. Int J Radiat Oncol Biol Phys 2009;75: 1111–1118.
5. Schisano G, Tovi D. Clivus chordomas. Neurochirurgia (Stuttg) 1962;5:99–120.
6. Bonneville F, Savatovsky J, Chiras J. Imaging of cerebellopontine angle lesions: an update. Part 2: intra-axial lesions, skull base lesions that may invade the CPA region, and non-enhancing extra-axial lesions. Eur Radiol 2007;17:2908–2920.
7. Feigl GC, Bundschuh O, Gharabaghi A, et al. Evaluation of a new concept for the management of skull base chordomas and chondrosarcomas. J Neurosurg 2005;102: 165–170.
8. Burger PC, Makek M, Kleinhues P. Tissue polypeptide antigen staining of the chordoma and notochordal remnants. Acta Neuropathol 1986;70:269–272.
9. Neff B, Sataloff RT, Storey L, et al. Chondrosarcoma of the skull base. Laryngoscope 2002;112:134–139.
10. Evans HL, Ayala AG, Romsdahl MM. Prognostic factors in chondrosarcoma of bone: a clinicopathologic analysis with emphasis on histologic grading. Cancer 1977; 40:818–831.
11. Cho YH, Kim JH, Khang SK, et al. Chordomas and chondrosarcomas of the skull base: comparative analysis of clinical results in 30 patients. Neurosurg Rev 2008;31: 35–43.
12. Samii A, Gerganov V, Herold C, et al. Surgical treatment of skull base chondrosarcomas. Neurosurg Rev 2009;32: 67–75.
13. Smolders D, Wang X, Drevelengas A, et al. Value of MRI in diagnosis of non-clival, non-sacral chordoma. Skeletal Radiol 2003;32:343–350.
14. Yeom KW, Lober RM, Mobley BC, et al. Diffusion-weighted MRI: distinction of skull base chordoma from chondrosarcoma. Am J Neuroradiol 2013;34: 1056–1061.
15. Ginat DT, Mangla R, Yeaney G, et al. Diffusion-weighted imaging for differentiating benign from malignant skull lesions and correlation with cell density. Am J Roentgenol 2012;198:W597–W601.
16. Weber DC, Rutz HP, Bolsi A, et al. Spot scanning proton therapy in the curative treatment of adult patients with sarcoma: the Paul Scherrer institute experience. Radiat Oncol Biol Phys 2007;69:865–871.
17. Patel MR, Siewert B, Warach S, et al. Diffusion and perfusion imaging techniques. Magn Reson Imaging Clin N Am 1995;3:425–438.
18. Stejskal E, Tanner J. Spin diffusion measurements: spin-echos in the presence of a time-dependent field gradient. J Chem Phys 1965;42:288–292.
19. Pamir MN, Ozduman K. Analysis of radiological features relative to histopathology in 42 skull-base chordomas and chondrosarcomas. Eur J Radiol 2006;58: 461–470.
20. Heffelfinger MJ, Dahlin DC, MacCarty CS, et al. Chordomas and cartilaginous tumors at the skull base. Cancer 1973;32:410–420.
21. Almefty K, Pravdenkova S, Colli BO, et al. Chordoma and chondrosarcoma: similar, but quite different, skull base tumors. Cancer 2007;110:2457–2467.
22. Oot RF, Melville GE, New PF, et al. The role of MR and CT in evaluating clival chordomas and chondrosarcomas. Am J Roentgenol 1988;151:567–575.
23. Crockard HA, Cheeseman A, Steel T, et al. A multidisciplinary team approach to skull base chondrosarcomas. J Neurosurg 2001;95:184–189.
24. Crockard HA, Steel T, Plowman N, et al. A multidisciplinary team approach to skull base chordomas. J Neurosurg 2001;95:175–183.
25. Ahlhelm F, Schneider G, Backens M, et al. Time course of the apparent diffusion coefficient after cerebral infarction. Eur Radiol 2002;12:2322–2329.
26. Hagen T, Alhelm F, Reiche W. Apparent diffusion coefficient in vasogenic edema and reactive astrogliosis. Neuroradiology 2007;49:921–926.
27. Goudarzi B, Kishimoto R, Komatsu S, et al. Detection of bone metastases using diffusion weighted magnetic resonance imaging: comparison with (11)C-methionine PET and bone scintigraphy. Magn Reson Imaging 2010;28: 372–379.
28. Abdel Razek A, Mossad A, Ghonim M. Role of diffusion-weighted MR imaging in assessing malignant versus benign skull-base lesions. Radiol Med 2011;116:125–132.
29. Hayashida Y, Hirai T, Yakushiji T, et al. Evaluation of diffusion-weighted imaging for the differential diagnosis of poorly contrast-enhanced and T2-prologed bone masses: initial experience. J Magn Reson Imaging 2006; 23:377–382.
30. Hoogendam JP, Klerkx WM, de Kort GA, et al. The influence of the b-value combination on apparent diffusion coefficient based differentiation between malignant and benign tissue in cervical cancer. J Magn Reson Imaging 2010;32:376–382.